Supplementary Material for:

Revisiting the electron microprobe method of spinel-olivine-orthopyroxene oxybarometry applied to spinel peridotites

Fred A Davis*[1,2], Elizabeth Cottrell[1], Suzanne K Birner[1,3], Jessica M Warren[4], Oscar G Lopez[1]

[1]National Museum of Natural History, Smithsonian Institution, Washington, DC 20560, USA

[2]Department of Earth and Environmental Sciences, University of Minnesota Duluth, Duluth, MN 55812, USA

[3]Department of Geological Sciences, Stanford University, Stanford, CA 94305, USA

[4]Department of Geological Sciences, University of Delaware, Newark, DE 19716, USA

*corresponding author, email: fdavis@d.umn.edu; tel: 1-218-726-8331

S1. Supplementary analytical methods

We analyzed major element compositions of minerals by WDS analysis by measuring K_α peaks of the following elements: SiO_2, TiO_2, Al_2O_3, Cr_2O_3, FeO* (ΣFe calculated as FeO), MnO, MgO, CaO, Na_2O, and NiO with a 15 kV accelerating voltage and 40 nA beam current. We used the Armstrong/Love-Scott ZAF procedure for matrix correction (Armstrong 1988). For olivine and spinel, we used a focused beam (~1 µm dia.) and for orthopyroxene a 40x48 µm raster. We chose primary standards (Table 1) compositionally similar to our unknowns (Jarosewich et al. 1980). We selected peak positions for each element at the beginning of each analytical session by performing a wavelength scan in the region of the peak. We performed the peaking operation using the same standard samples used for the primary standardization for each element (Table 1), except Ni, which we peaked on $Fe_{90}Ni_{10}$ alloy. We counted both peaks and backgrounds at each analytical point.

S2. Selection criteria for the correction and validation sets

From among the Wood spinels analyzed in sessions S1-S3, we selected IO5657, Vi314-5, IM8703, DB8803-3, BAR8601-10, MO4334-14, and KLB8320 to be the correction set. We chose these samples because they span the entire available range of oxidation states (Mössbauer $Fe^{3+}/\Sigma Fe$ = 0.058 to 0.32) and compositions (Cr# = 0.04 to 0.58; MgO = 14.8 to 21.4 wt.%), as shown in Fig. 2. Each of the correction set spinels have sample average uncorrected EPMA $Fe^{3+}/\Sigma Fe$ ratios within ±0.02 of the Mössbauer $Fe^{3+}/\Sigma Fe$ ratios reported by the Wood group (Fig. 1). We checked for intergranular heterogeneity by calculating the difference between grain-average and sample-average $Fe^{3+}/\Sigma Fe$ ratios of each sample. All correction set grain-average $Fe^{3+}/\Sigma Fe$ ratios are within ±0.03 of their sample averages, except IO5657 (±0.04), which was selected for the correction set despite moderate intergranular heterogeneity because there is a relative dearth of samples with Mössbauer $Fe^{3+}/\Sigma Fe$ ratios < 0.10.

We selected PS211, PS212, KLB8304, MBR8313, Vi314-58, OC231350 (Sessions A1-A4 only), and IO5650 (sessions B1-B4 only) for the validation set. The selection criteria for these samples were similar to those for the correction set but with wider tolerance for $\Delta Fe^{3+}/\Sigma Fe^{Möss\text{-}EPMA}$. Each of the validation set spinels have sample average uncorrected EPMA $Fe^{3+}/\Sigma Fe$ ratios within ±0.035 of the Mössbauer $Fe^{3+}/\Sigma Fe$ ratios reported by the Wood group (Fig. 1). All validation set grain average $Fe^{3+}/\Sigma Fe$ ratios are within ±0.03 of their sample averages, except OC231350 (±0.05).

S3. V, Co, and Zn in peridotite-hosted spinels in the GEOROC database

We examined geochemical data for spinels contained in the GEOROC database by downloading the pre-compiled file SPINELS.csv (http://georoc.mpch-mainz.gwdg.de/georoc/, accessed 30 June 2016). We first filtered the dataset for only those samples with a “rock name” given as

peridotite, lherzolite, harzburgite, or dunite. 139 of these samples had both major and trace element data. A smaller subset of 42 had values for V, Co, and Zn. These 42 samples are plotted in Suppl. Fig. S1 to demonstrate correlations in the data. V is correlated with both Co ($r^2 = 0.54$) and Zn ($r^2 = 0.33$).

S4. Calculations to demonstrate the effect of the W&V89 correction on biased data sets

We demonstrate the effectiveness of the W&V89 correction in addressing different analytical biases by using simulated data to perturb the analysis of individual elements and then observing how the W&V89 correction responds. In Suppl. Fig. S2, we show idealized compositions of the correction set spinels and two example unknowns and the effects of biases in the analysis of Al and Mg. To generate the simulated data in Suppl. Fig. S2, we derived idealized compositions of the correction set spinels, validation set spinel Vi314-58, and spinel from BMRG08-98-2-2. We adjusted the average compositions of the correction set spinels and Vi314-58 determined in Sessions S1-S3 (Table 2) by changing the value of total Fe (FeO*) until the $Fe^{3+}/\Sigma Fe$ ratio calculated from the stoichiometry matched the $Fe^{3+}/\Sigma Fe$ ratio determined by Mössbauer (Suppl. Table S6). To plot Tonga spinel BMRG08-98-2-2 on Suppl. Fig. S2, we applied this same procedure to the average BMRG08-98-2-2 composition reported in Table 4, and treated the average $Fe^{3+}/\Sigma Fe$ ratio determined in this study (Table 4) as its true $Fe^{3+}/\Sigma Fe$ ratio.

To simulate analytical biases, we multiplied the element with the biased analysis in each sample by a bias factor. For example, to arrive at the compositions in Suppl. Fig. S2a, in which a 5% over-analysis of Al_2O_3 was simulated, we multiplied all Al_2O_3 concentrations by 1.05. This is approximately equivalent to a +5% error in the intensity ratio for Al. We then corrected the

spinel compositions in each of these simulations using the W&V89 method. All calculated compositions presented in Suppl. Fig. S2 are given in Suppl. Table S6.

Suppl. Fig. S2a and S2b show the effects of a 5% over-analysis of Al_2O_3. The uncorrected EPMA $Fe^{3+}/\Sigma Fe$ ratios all fall well below the 1:1 line (Suppl. Fig. S2a). There is also increased scatter in the data because samples with higher Al_2O_3 concentrations are more severely affected by the analytical bias (shown by arrows). The W&V89 correction brings these data closer to agreement with the Mössbauer $Fe^{3+}/\Sigma Fe$ ratios (Suppl. Fig. S2b). This is not surprising because the correction directly involves Al_2O_3. Suppl. Fig. S2c and S2d show the effects of a 5% under-analysis of MgO. Again, the uncorrected $Fe^{3+}/\Sigma Fe$ ratios are scattered and plot well below the 1:1 line (Suppl. Fig. S2c), and the correction results in $Fe^{3+}/\Sigma Fe$ ratios more closely in agreement with the Mössbauer ratios (Suppl. Fig. S2d). Although the offset in the uncorrected compositions is due only to bias in the MgO measurement, the W&V89 correction adjusts for this bias because spinel MgO concentrations correlate with Cr# (Fig. 8).

The W&V89 correction is less effective for a spinel that does not plot on the MgO-Cr# trend. The spinel in Tonga sample BMRG08-98-2-2 plots well off the Cr#-MgO trend of the correction set spinels (Fig. 8). Suppl. Fig. S2a shows that bias in the measurement of Al_2O_3 leads to only a small change in the $Fe^{3+}/\Sigma Fe$ ratio of BMRG08-98-2-2 because it is has a relatively low Al_2O_3 concentration. The correction, appropriately, makes only a small adjustment to its $Fe^{3+}/\Sigma Fe$ ratio (Suppl. Fig. S2b). When the MgO analysis is biased, there is again only a small change in the $Fe^{3+}/\Sigma Fe$ ratio of BMRG08-98-2-2 because it also has relatively low MgO (Suppl. Fig. S2c). Under these conditions, the W&V89 correction overcorrects for the bias because BMRG08-98-2-2 has much lower MgO at a given Cr# than do the correction set spinels (Fig. 8). Hence, corrected BMRG08-98-2-2 plots nearly as far above the 1:1 line after correction (+0.019) as it

did below the line before correction (-0.025). Although a difference from its true $Fe^{3+}/\Sigma Fe$ ratio of 0.019 may seem small in an absolute sense, it is nearly twice that expected for such an Fe-rich sample (FeOT = 22.9 wt.%) as calculated from Eq. 3 ($1\sigma_3 = 0.010$). We would expect a less Fe-rich or more Mg-rich spinel to see even larger deviations from its true $Fe^{3+}/\Sigma Fe$ ratio when subjected to a similar bias in MgO.

Consistent with our data simulations, repeated analyses of BMRG08-98-2-2 spinel show equivalent intersession variability in the $Fe^{3+}/\Sigma Fe$ ratio (represented by the magnitude of 1σ) for uncorrected and corrected $Fe^{3+}/\Sigma Fe$ ratios. We contrast this with our results for all validation set spinels and Hawaiian spinels, where 1σ is less for corrected $Fe^{3+}/\Sigma Fe$ ratios compared to uncorrected ratios (Table 4). The practical implication is that analyses of spinels that do not plot on the same compositional trend as the Wood spinels may be subject to diminished precision; however, we are not currently able to quantify this effect.

S5. The calculation of magnetite activity in spinel ($a^{spl}_{Fe_3O_4}$)

Several parameterizations are available to calculate magnetite activity in spinel, $a^{spl}_{Fe_3O_4}$ (O'Neill and Wall 1987; Mattioli and Wood 1988; Nell and Wood 1991; Sack and Ghiorso 1991a, 1991b). In an experimental test of the oxybarometer (eq. 4), Wood (1990) explored the consequences of applying several of the spinel activity models that were available. He found that the model of Mattioli and Wood (1988) resulted in differences between calculated and experimental f_{O2} (Δf_{O2}) that varied systematically with the Cr# of spinel. The models of O'Neill and Wall (1987) and Nell and Wood (1991) both lacked any compositional dependence to Δf_{O2}, but both resulted in systematically lower calculated f_{O2} than the known f_{O2} of the experimental gas mixture. Wood (1990) recommended the use of the Nell-Wood activity model because it

gave the smallest offset of Δf_{O2} = -0.35 log units. Herd (2008) recalculated f_{O2} in the experiments of Wood (1990) by applying $a^{spl}_{Fe_3O_4}$ calculated using the MELTS Supplemental Calculator (Sack and Ghiorso 1991a, 1991b; http://melts.ofm-research.org/CalcForms/index.html). He found that the offset between calculated and experimental f_{O2} decreased to Δf_{O2} = -0.07 log units when using this parameterization of $a^{spl}_{Fe_3O_4}$.

We adopt the MELTS Supplemental Calculator for calculating $a^{spl}_{Fe_3O_4}$, with an important change to the conversion of oxide compositions to spinel components. The MELTS Supplemental Calculator requires input of spinel end-member components: chromite – $FeCr_2O_4$, hercynite – $FeAl_2O_4$, magnetite – Fe_3O_4, spinel – $MgAl_2O_4$, and ulvöspinel – $TiFe_2O_4$. The website allows the user to enter spinel compositions as weight percent oxides, and the calculator will output the spinel end-member compositions. That calculation proceeds by first recalculating the Fe^{3+}/Fe^{2+} ratio based on stoichiometry, then assigining Mg to spinel, Cr to chromite, Ti to ulvöspinel, Fe^{3+} to magnetite and the remaining Fe to hercynite. This procedure eliminates any information about $Fe^{3+}/\Sigma Fe$ ratio provided by application of the W&V89 correction, effectively reproducing the stoichiometric calculation but with less information. This method also systematically underestimates the magnetite component because minor divalent cations that are present in spinel (i.e., Mn and Ni) are left out of the calculation, while all common trivalent cations are represented. Instead, we calculated spinel components in a separate spreadsheet using Fe3+/Fe2+ ratios determined from our analysis and correction. We assigned cations to spinel components following the same method described above and then normalized the sum of components to one. This method preserves the $Fe^{3+}/\Sigma Fe$ ratio and Mg# of the original microprobe analysis, while increasing Cr# by only 1-3% relative to the original analysis. We

recalculated $a_{Fe_3O_4}^{spl}$ in the experiments of Wood (1990) following this method, and found that the resulting average difference between calculated and experimental f_{O2} is diminished to Δf_{O2} = -0.03 log units. Although this is a small change from the result reported by Herd (2008), this represents the closest fit between calculated and experimental f_{O2} of any method. As discussed below, and by Wood and Virgo (1989), uncertainty in $a_{Fe_3O_4}^{spl}$ is the greatest contributor to uncertainty in the calculation of f_{O2}.

S6. Uncertainty in the f_{O2} calculation due to precision in the analysis of olivine and orthopyroxene and the estimation of pressure and temperature of equilibration

We isolate the effect of each variable by using the average mineral compositions of our analyses of Hawaiian xenolith sample 114923-57 (Tables 3 and 4) as a baseline and changing the value of each compositional variable over a range relevant to natural peridotites (i.e., $Mg\#^{ol}$ = 0.85 to 0.95, $(X_{Fe}^{M1} \cdot X_{Fe}^{M2})^{opx}$ = 0.002-0.025, $log a_{Fe_3O_4}^{spl}$=-3.4 to -1.2).

We estimate the precision of our measurement of $Mg\#^{ol}$ from repeated analysis of the Springwater Meteorite olivine standard (Jarosewich et al. 1980), used as a secondary standard over four analytical sessions (n=42 measurements, Suppl. Table S7). This set of analyses has an average $Mg\#^{ol}$ = 0.8251 ± 0.0014 (1σ), which is within error of the published value of 0.824 (Jarosewich et al. 1980). Suppl. Fig. S3a shows that relative f_{O2} increases with $Mg\#^{ol}$. Given our stated precision for $Mg\#^{ol}$ of ±0.0014, the uncertainty in relative f_{O2} contributed by the olivine analysis varies from ±0.04 log units at $Mg\#^{ol}$=0.85 to ±0.14 log units at $Mg\#^{ol}$=0.95. This uncertainty can be approximated by a third-order polynomial:

$$1\sigma_{S1} = 103.59x^3 - 270.14x^2 + 235.24x - 68.353 \quad \text{(S1)}$$

where is $1\sigma_{S1}$ describes the magnitude of two standard deviations in the uncertainty on the calculation of log f_{O2} contributed by the olivine analysis, and x is $Mg\#^{ol}$.

We estimate the precision of our measurement of $(X_{Fe}^{M1} \cdot X_{Fe}^{M2})^{opx}$ from repeated analysis of the Johnstown Meteorite hypersthene standard (Jarosewich et al. 1980), also used as a secondary standard over four analytical sessions (n = 42 measurements, Suppl. Table S8). This set of analyses has an average $(X_{Fe}^{M1} \cdot X_{Fe}^{M2})^{opx} = 0.0518 \pm 0.0017$ (1σ), compared to 0.052 calculated from the published composition (Jarosewich et al. 1980). Because $(X_{Fe}^{M1} \cdot X_{Fe}^{M2})^{opx}$ is directly tied to the measurement of FeO* (ΣFe calculated as FeO) in the pyroxene, we expect that precision should scale roughly to the concentration of FeO*. We assume then that 1σ for our $(X_{Fe}^{M1} \cdot X_{Fe}^{M2})^{opx}$ measurements of unknown orthopyroxene is 7% relative. The effect of orthopyroxene composition on relative f_{O2} (Suppl. Fig. S3b) is to increase relative f_{O2} with increasing orthopyroxene Fe concentration (opposite to the effect of olivine composition). The uncertainty on relative f_{O2} due to the orthopyroxene analysis is ±0.04 log units.

The covariation of olivine and orthopyroxene Mg/Fe ratios in peridotites will dampen the competing compositional effects of olivine and orthopyroxene on calculated f_{O2}. Suppl. Fig. S3c shows the relationship between relative f_{O2} when olivine and orthopyroxene compositions covary but other variables are held constant. In this simplified calculation, $X_{Fe}^{M1,opx} = X_{Fe}^{M2,opx} = (1-Mg\#^{ol})$. The result is that calculated f_{O2} increases with $Mg\#^{ol}$, but the effect is muted compared to the effect of holding orthopyroxene composition constant while changing $Mg\#^{ol}$. Although compositional covariance limits the leverage of the silicate phases on the calculation of f_{O2}, uncertainty in the olivine and orthopyroxene analyses still contribute additively to uncertainty on the f_{O2} calculation if the two silicates are analyzed in separate analytical sessions.

We calculate $a_{Fe_3O_4}^{spl}$ using the MELTS Supplemental Calculator (Sack and Ghiorso 1991a, 1991b, http://melts.ofm-research.org/CalcForms/index.html). Because this is a complex calculation, we cannot easily propagate our uncertainty in spinel $Fe^{3+}/\Sigma Fe$ ratio through the calculation of $a_{Fe_3O_4}^{spl}$. Instead, we have determined an empirical relationship between spinel $Fe^{3+}/\Sigma Fe$ ratio and $a_{Fe_3O_4}^{spl}$ calculated using the MELTS Supplemental Calculator.

To learn how calculated $a_{Fe_3O_4}^{spl}$ varies with spinel $Fe^{3+}/\Sigma Fe$ ratio, we calculated series of hypothetical spinel compositions based on three natural spinel compositions from this study (114885-3, 114923-41, and BMRG08-98-2-2; Table 4) at two different temperatures (740 °C, 1150 °C). These spinels differ in major element compositions (114885-3: Cr# = 0.424; 114923-41: Cr# = 0.122; BMRG08-98-2-2: Cr# = 0.676). For each of these spinel compositions, we calculated a series of similar spinel compositions with a constant Cr# and a range of $Fe^{3+}/\Sigma Fe$ ratios from 0 to 0.40. We achieved this by setting the molar proportion of the magnetite component to a specified value, starting at 0 and increasing in increments of 0.002, and holding the ratios of the other spinel components constant with respect to one another. The calculated spinel compositions retain the Cr# of the base spinel composition (either 114885-3, 114923-41, or BMRG08-98-2-2, Table 4). The Mg# ($Mg/(Mg+Fe^{2+})$) in the calculated spinel compositions varies; although, it is over a small range (calculations based on 114885-3 have Mg# from 0.65-0.68; 114923-41 Mg# from 0.80-0.82; BMRG08-98-2-2 Mg# from 0.43-0.46). We calculated $a_{Fe_3O_4}^{spl}$ for each of these model compositions using the MELTS Supplemental Calculator. For each composition and temperature, the resulting range of $a_{Fe_3O_4}^{spl}$ can be related to the spinel $Fe^{3+}/\Sigma Fe$ ratio by a function with the form:

198 $$\log\left(a_{Fe_3O_4}^{spl}\right) = \ln(\mathrm{Fe^{3+}}/\Sigma\mathrm{Fe})^{spl} + C \quad \text{(S2)}$$

199 where $(\mathrm{Fe^{3+}}/\Sigma\mathrm{Fe})^{spl}$ is the spinel $\mathrm{Fe^{3+}}/\Sigma\mathrm{Fe}$ ratio and *C* is a constant. The calculated $a_{Fe_3O_4}^{spl}$

200 series and fits are presented in Suppl. Fig. S4. Functions of the form given in Eq. S1 have values

201 of $R^2 = 1 - (\Sigma(y\text{-}y_{model})^2/\ \Sigma(y\text{-}y_{mean})^2)$ between 0.986 and 0.997.

202 If a function with the form of Eq. S2 can be found to fit any combination of spinel composition

203 and temperature, then we can describe a general expression to estimate uncertainty in $a_{Fe_3O_4}^{spl}$

204 resulting from uncertainty in the measurement of the $\mathrm{Fe^{3+}}/\Sigma\mathrm{Fe}$ ratio. The difference between

205 $\log\left(a_{Fe_3O_4}^{spl}\right)$ of a measured spinel composition and the value at one standard deviation in the

206 $\mathrm{Fe^{3+}}/\Sigma\mathrm{Fe}$ ratio (σ_3 in the main text) is given by:

207 $$\Delta\log\left(a_{Fe_3O_4}^{spl}\right) = \ln\left(\frac{\mathrm{Fe^{3+}}}{\Sigma\mathrm{Fe}} \pm \sigma_3\right) + C - \ln\left(\frac{\mathrm{Fe^{3+}}}{\Sigma\mathrm{Fe}}\right) - C \quad \text{(S3)}$$

208 The constant, *C*, drops out, so that as long as a function of the form of Eq. S1 exists, we do not

209 need to determine the value of the constant. Eq. S3 then reduces to:

210 $$\Delta\log\left(a_{Fe_3O_4}^{spl}\right) = \ln\left(1 \pm \frac{\sigma_3}{\mathrm{Fe^{3+}}/\Sigma\mathrm{Fe}}\right) \quad \text{(S4)}$$

211 which can be used to estimate positive and negative uncertainty in $\log\left(a_{Fe_3O_4}^{spl}\right)$.

212 The effects of temperature uncertainty on calculated f_{O2} are shown in Suppl. Fig. S5, again using

213 Hawaiian xenolith 114923-57 as a base composition. Increasing temperature leads to a decrease

214 in calculated f_{O2} (Suppl. Fig. S5a). Suppl. Fig. S5b shows how f_{O2} of a different peridotite

215 sample, 114923-41, with lower Cr# is affected by changes in temperature over the same

216 temperature range. Decreasing Cr# increases the T-dependency of $a_{Fe_3O_4}^{spl}$ such that the overall T-

217 f_{O2} relationship is magnified, and the uncertainty in f_{O2} associated with temperature increases. If
218 we break the temperature dependence into its component parts, we see that the contribution of
219 temperature to Eq. 4 (main text) actually acts to increase calculated f_{O2} as temperature increases
220 (Suppl. Fig S5c), and the overall effect of decreasing f_{O2} with increasing temperature is caused
221 by the strong temperature-dependence of $a_{Fe_3O_4}^{spl}$.

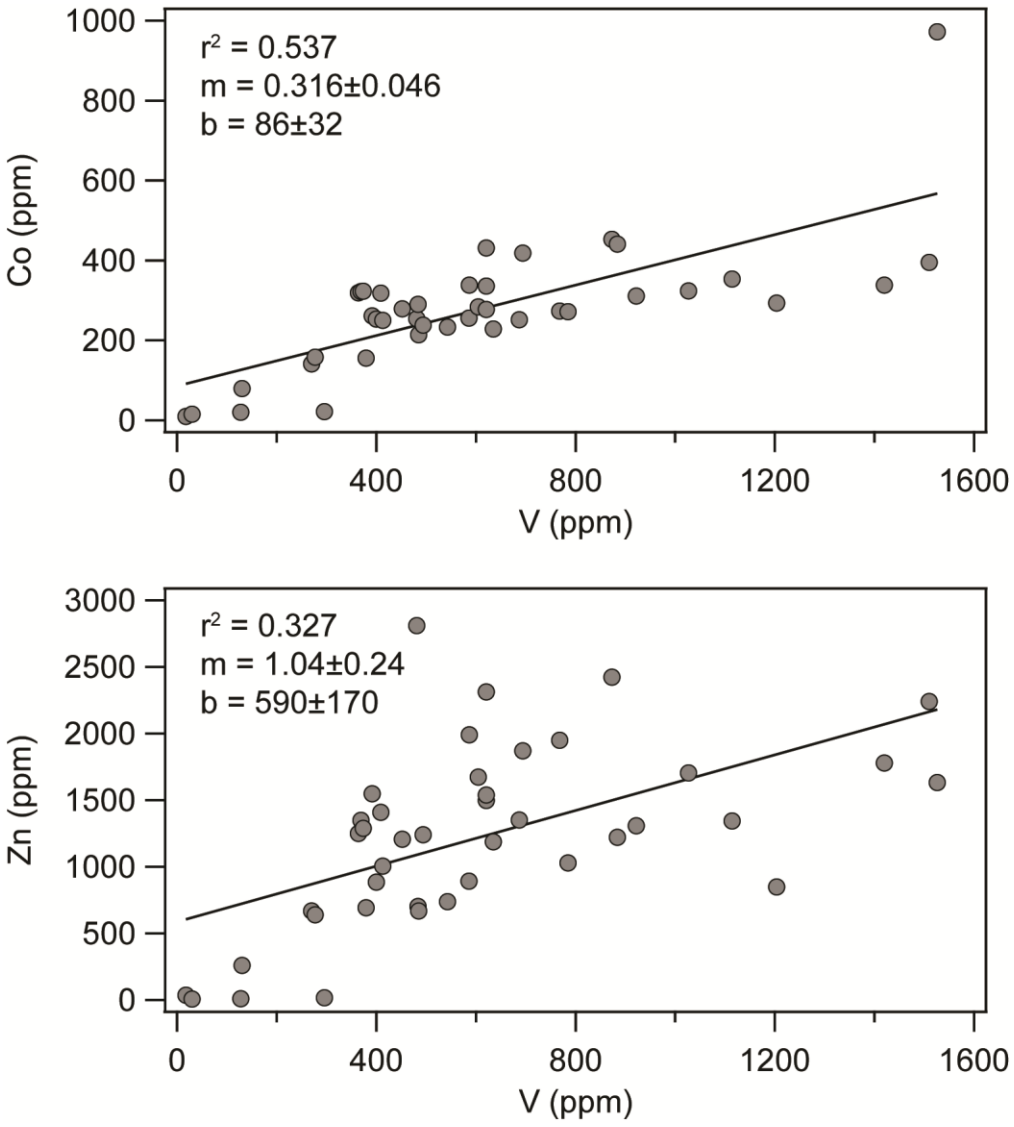

Supplementary Figure S1. Concentrations of V, Co, and Zn in peridotite-hosted spinels from GEOROC database. Data are originally from Jan and Howie (1981), Norman (1998), Glaser et al. (1999), Karmalkar et al. (2000), van Achterbergh et al. (2001), Zheng et al. (2001), Rehfeldt et al. (2007), Bascou et al. (2008), Harvey et al. (2012), Lu et al. (2013).

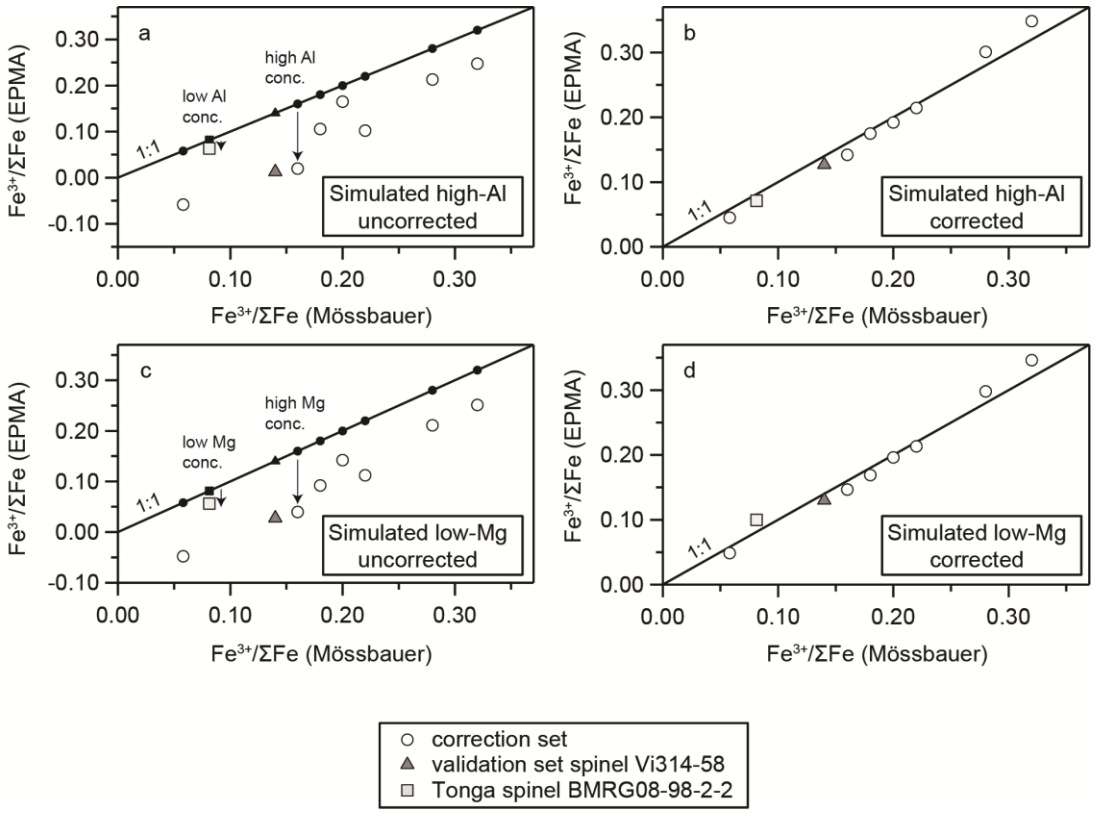

227

228 **Supplementary Figure S2: Simulated EPMA data to demonstrate correction of analytical**
229 **bias in Al_2O_3 and MgO.** Small black symbols (a, c) show idealized compositions of the
230 correction set spinels, validation set spinel Vi314-58, and Tonga spinel BMRG08-98-2-2. An
231 analytical session in which the Al_2O_3 measurement is biased by +5% leads to underestimation of
232 $Fe^{3+}/\Sigma Fe$ ratios by EPMA (a); samples with higher Al_2O_3 concentration are more strongly
233 affected by bias. The W&V89 correction improves agreement between EPMA measurements
234 and true $Fe^{3+}/\Sigma Fe$ ratios when Al_2O_3 is biased (b). An analytical session in which the MgO
235 measurement is biased by -5% also leads to underestimation of $Fe^{3+}/\Sigma Fe$ ratios by EPMA (c).
236 Although it is uses only Cr# and $\Delta Fe^{3+}/\Sigma Fe^{Möss\text{-}EPMA}$, the W&V89 correction still improves
237 agreement between EPMA measurements and true $Fe^{3+}/\Sigma Fe$ ratios when MgO is biased (d).
238 Tonga sample BMRG08-98-2-2 is over-corrected by the W&V89 method when MgO is biased
239 because it plots off of the Cr#-MgO trend defined by the correction set spinels (Fig. 8).

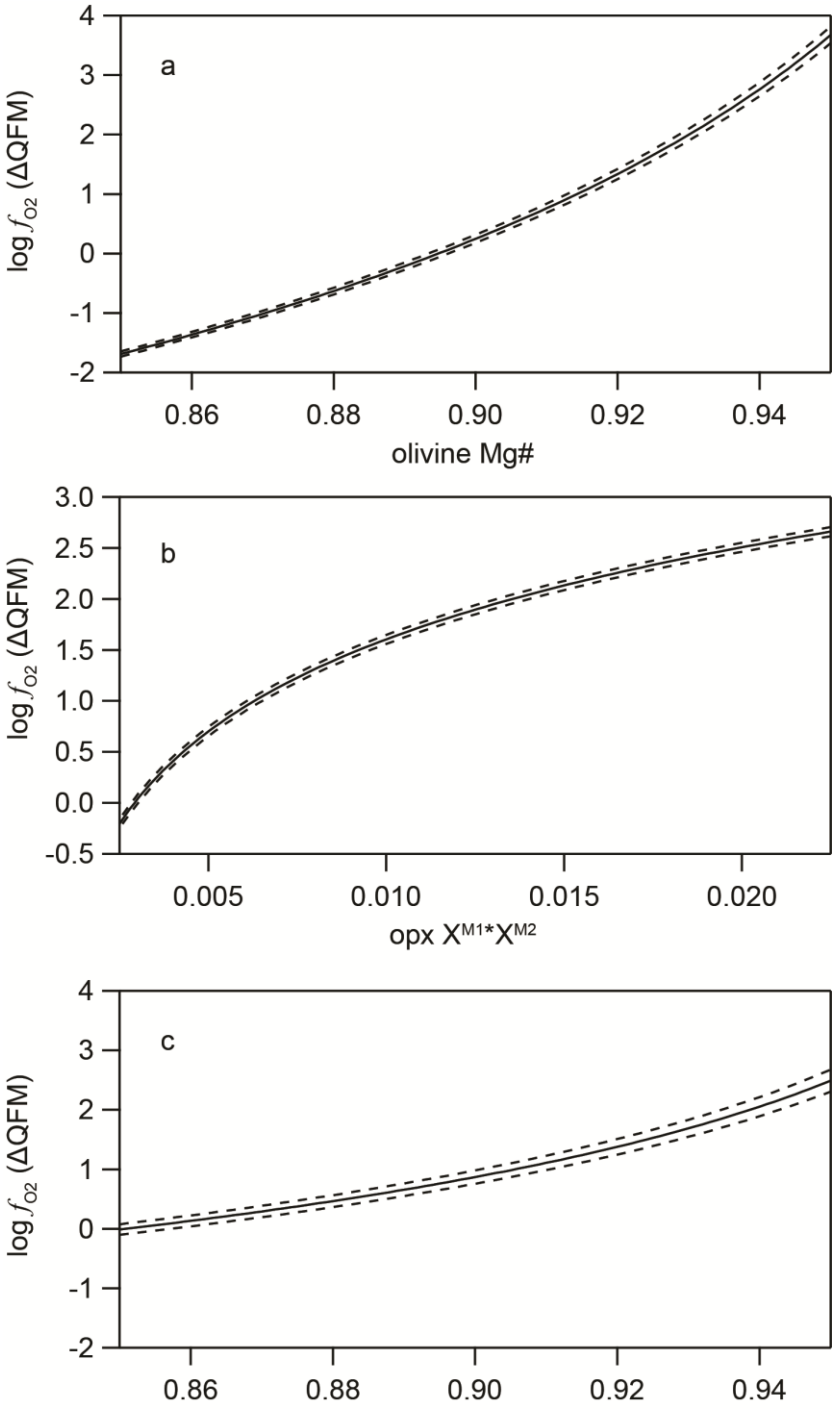

240

241 **Supplementary Figure S3: Effects of olivine forsterite content and orthopyroxene Fe site**
242 **occupancy on the calculation of relative f_{O2}.** Calculated logf_{O2} relative to the quartz-fayalite-
243 magnetite buffer (ΔQFM, Frost 1991 calibration) using all input parameters from sample

114923-57 at 1038 °C and 1.5 GPa and varying the Mg# of coexisting olivine between 0.85 and 0.95 (a). The dashed lines show ±1σ error on the EMP measurement. This uncertainty can be approximated using the polynomial expression in Eq. S1. Calculated logf_{O2} (ΔQFM) after varying the value of $(X_{Fe}^{M1} \cdot X_{Fe}^{M2})^{opx}$ and holding $Mg\#^{ol}$ constant (b). The uncertainty contributed by the orthopyroxene analysis is ±0.04 log units. Calculated f_{O2} over the same range of olivine composition while allowing for covariation of olivine and orthopyroxene compositions (c). For this calculation, $X_{Fe}^{M1,opx} = X_{Fe}^{M2,opx} = (1\text{-}Mg\#^{ol})$.

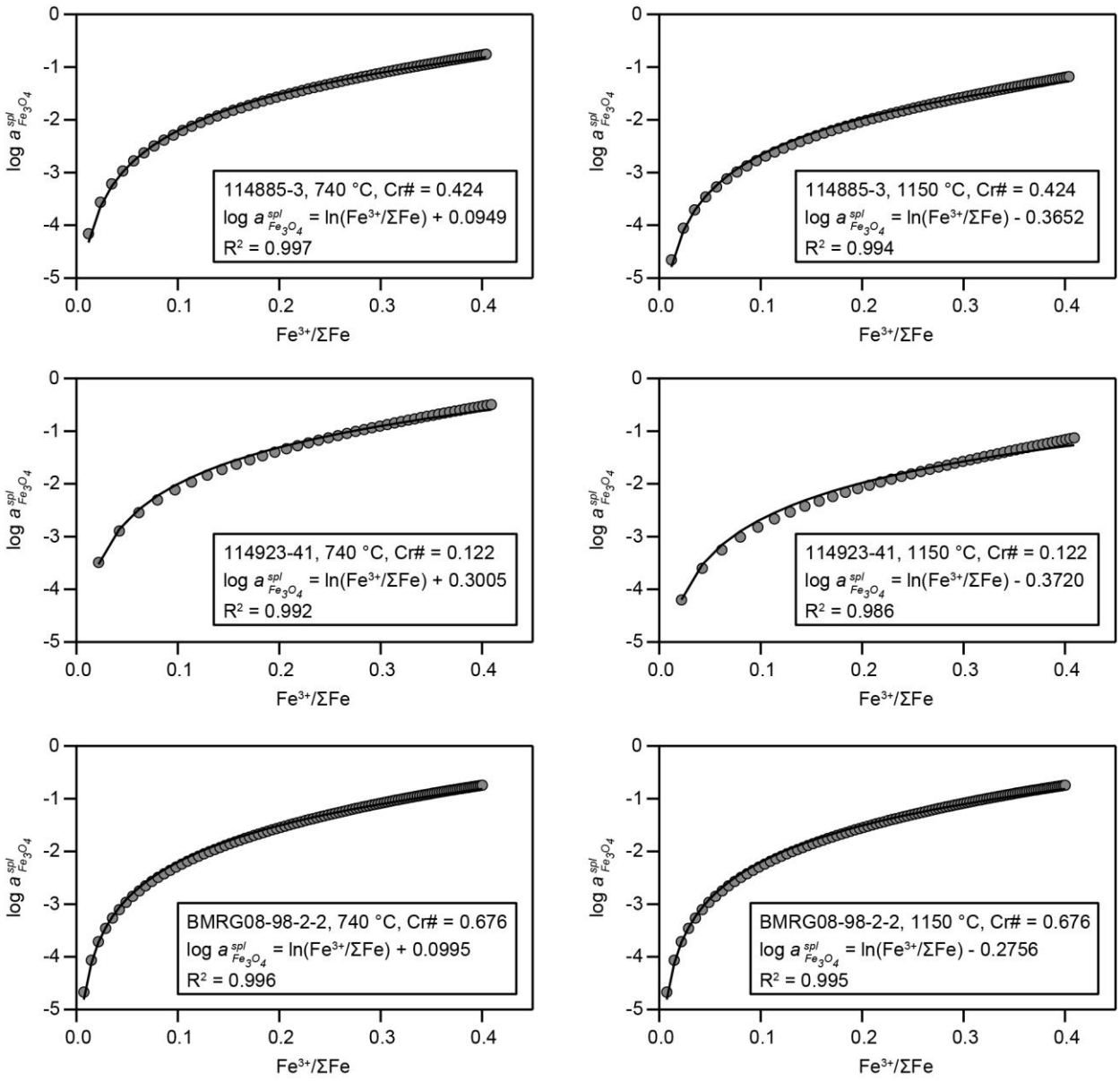

Supplementary Figure S4. Relationship between spinel $Fe^{3+}/\Sigma Fe$ ratio and $a_{Fe_3O_4}^{spl}$ calculated using the MELTS Supplemental Calculator. Circles show the calculated spinel compositions based on Hawaiian spinel samples 114885-3 and 114923-41 and Tonga sample BMRG08-98-2-2. The black curves are fits of the functional form given by Eq. S2. We describe in the text above the method for calculating spinel compositions with variable $Fe^{3+}/\Sigma Fe$ ratios but leaving other compositional ratios nearly constant. R^2 is the coefficient of determination, calculated as described above.

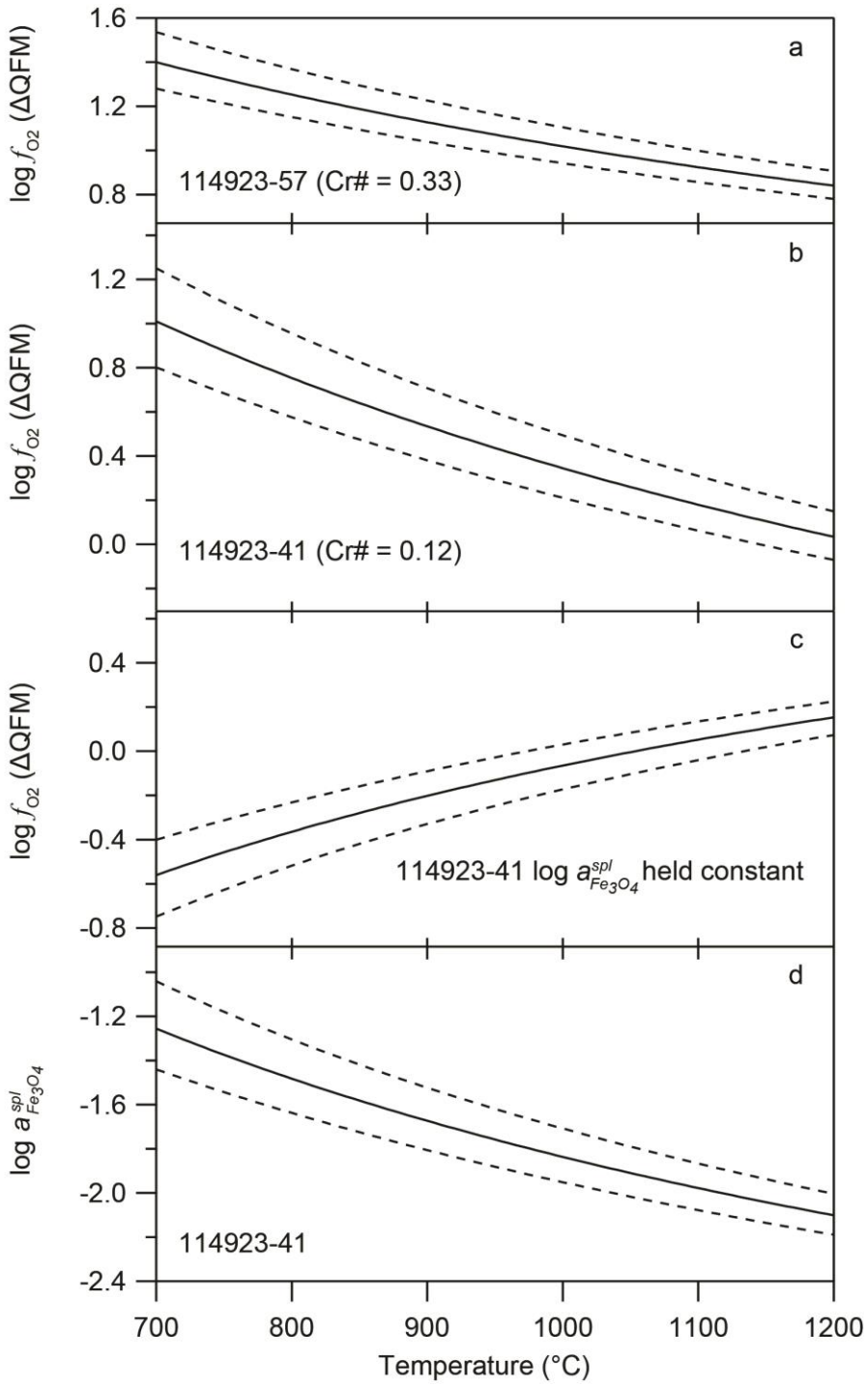

Supplementary Figure S5: Effect of temperature on the calculation of relative f_{O2}. Calculated log f_{O2} (ΔQFM) as in Suppl. Fig. S3 but varying the temperature rather than any compositional variable (a). Dashed lines show uncertainty in temperature of ±80 °C.

Temperature effect calculated using the compositional data from sample 114923-41 (b), which has lower Cr# spinel (0.12) than 114923-57 (Cr#=0.33). This demonstrates the increased temperature-sensitivity of the relative f_{O2} calculation at lower Cr#, which leads to a larger temperature-derived uncertainty. The effect of varying temperature on the calculation of relative f_{O2} for sample 114923-41with $log a_{Fe_3O_4}^{spl}$ held constant at -2.04 (c). Variation in $log a_{Fe_3O_4}^{spl}$ for sample 114923-41 owing to changes in estimated temperature of equilibration (d).

References

Armstrong, J. (1988) Quantitative analysis of silicate and oxide minerals: comparison of Monte Carlo, ZAF and phi-rho-z procedures. Microbeam analysis, 23, 239–246.

Bascou, J., Delpech, G., Vauchez, A., Moine, B., Cottin, J.-Y., and Barruol, G. (2008) An integrated study of microstructural, geochemical, and seismic properties of the lithospheric mantle above the Kerguelen plume (Indian Ocean). Geochemistry, Geophysics, Geosystems, 9.

Frost, B.R. (1991) Introduction to oxygen fugacity and its petrologic importance. Reviews in Mineralogy and Geochemistry, 25, 1–9.

Glaser, S.M., Foley, S.F., and Günther, D. (1999) Trace element compositions of minerals in garnet and spinel peridotite xenoliths from the Vitim volcanic field, Transbaikalia, eastern Siberia. Lithos, 48, 263–285.

Harvey, J., Yoshikawa, M., Hammond, S.J., and Burton, K.W. (2012) Deciphering the trace element characteristics in Kilbourne Hole peridotite xenoliths: melt–rock interaction and metasomatism beneath the Rio Grande Rift, SW USA. Journal of Petrology, egs030.

Herd, C.D. (2008) Basalts as probes of planetary interior redox state. Reviews in Mineralogy and Geochemistry, 68, 527–553.

Jan, M.Q., and Howie, R. (1981) The mineralogy and geochemistry of the metamorphosed basic and ultrabasic rocks of the Jijal complex, Kohistan, NW Pakistan. Journal of Petrology, 22, 85–126.

Jarosewich, E., Nelen, J., and Norberg, J.A. (1980) Reference Samples for Electron Microprobe Analysis*. Geostandards Newsletter, 4, 43–47.

Karmalkar, N., Griffin, W., and O'REILLY, S.Y. (2000) Ultramafic xenoliths from Kutch, Northwest India: plume-related mantle samples? International Geology Review, 42, 416–444.

Lu, J., Zheng, J., Griffin, W.L., and Yu, C. (2013) Petrology and geochemistry of peridotite xenoliths from the Lianshan region: nature and evolution of lithospheric mantle beneath the lower Yangtze block. Gondwana Research, 23, 161–175.

Mattioli, G.S., and Wood, B.J. (1988) Magnetite activities across the MgAl2O4-Fe3O4 spinel join, with application to thermobarometric estimates of upper mantle oxygen fugacity. Contributions to Mineralogy and Petrology, 98, 148–162.

Nell, J., and Wood, B.J. (1991) High-temperature electrical measurements and thermodynamic properties of Fe3O4-FeCr2O4-MgCr2O4-FeAl2O4 spinels. American Mineralogist, 76, 405–426.

Norman, M.D. (1998) Melting and metasomatism in the continental lithosphere: laser ablation ICPMS analysis of minerals in spinel lherzolites from eastern Australia. Contributions to Mineralogy and Petrology, 130, 240–255.

O'Neill, H.S.C., and Wall, V. (1987) The Olivine—Orthopyroxene—Spinel oxygen geobarometer, the nickel precipitation curve, and the oxygen fugacity of the Earth's Upper Mantle. Journal of Petrology, 28, 1169–1191.

Rehfeldt, T., Jacob, D.E., Carlson, R.W., and Foley, S.F. (2007) Fe-rich dunite xenoliths from South African kimberlites: cumulates from Karoo flood basalts. Journal of Petrology, 48, 1387–1409.

Sack, R.O., and Ghiorso, M.S. (1991a) An internally consistent model for the thermodynamic properties of Fe- Mg-titanomagnetite-aluminate spinels. Contributions to Mineralogy and Petrology, 106, 474–505.

——— (1991b) Chromian spinels as petrogenetic indicators; thermodynamics and petrological applications. American Mineralogist, 76, 827–847.

van Achterbergh, E., Griffin, W.L., and Stiefenhofer, J. (2001) Metasomatism in mantle xenoliths from the Letlhakane kimberlites: estimation of element fluxes. Contributions to Mineralogy and Petrology, 141, 397–414.

Wood, B.J. (1990) An experimental test of the spinel peridotite oxygen barometer. Journal of Geophysical Research: Solid Earth, 95, 15845–15851.

Wood, B.J., and Virgo, D. (1989) Upper mantle oxidation state: Ferric iron contents of Iherzolite spinels by 57Fe Mössbauer spectroscopy and resultant oxygen fugacities. Geochimica et Cosmochimica Acta, 53, 1277–1291.

Zheng, J., O'Reilly, S.Y., Griffin, W., Lu, F., Zhang, M., and Pearson, N. (2001) Relict refractory mantle beneath the eastern North China block: significance for lithosphere evolution. Lithos, 57, 43–66.